Molecular Dynamics Simulation of Fe^{2+}(aq) and Fe^{3+}(aq)

Sami Amira,[†] Daniel Spångberg,[†] Michael Probst,[‡] and Kersti Hermansson*,[†]

Materials Chemistry, The Ångström Laboratory, Uppsala University, Box 538, S-751 21 Uppsala, Sweden, and Institut für Ionenphysik, Leopold Franzens Universität, Technikerstrasse 25, A-6020 Innsbruck, Austria

Received: April 2, 2003; In Final Form: July 7, 2003

Molecular dynamics simulations of single-ion Fe^{2+}(aq) and Fe^{3+}(aq) solutions have been performed with two rigid-water models (SPC and SPC/E) and a newly constructed SPC-based flexible-water model (SPC+CCL). The SPC+CCL water model in combination with effective Fe^{2+} and Fe^{3+} ion−water potentials manages to reproduce many experimental structural and dynamical properties of the solutions. Special attention is given to the large ion-induced frequency shifts of the OH stretching bands, which are also well reproduced by the SPC+CCL model.

1. Introduction

Solvent structure and solvent exchange are important keys to understanding the dynamics of chemical reactions in solution. The motion of solvent molecules and the way they arrange themselves around reacting species critically affect the energetics and kinetics of the chemical reactions. The experimental determination of solvation structure and dynamics is generally not a trivial task; here computer simulations (Monte Carlo, molecular dynamics (MD)) can help provide precise molecular-level information. An extensive compilation by Ohtaki and Radnai[1] summarizes experimental and theoretical results for aqueous ionic solutions until 1993.

In this paper, we are concerned with the solvation structure and the ionic and molecular dynamics of dilute aqueous solutions of Fe^{2+} and Fe^{3+}. Previous theoretical studies of ferrous and ferric ions in aqueous solutions discuss solvation-shell structure,[2−7] ion and water diffusion,[7] hydrolysis,[8] charge-transfer reactions,[9−11] ion-pair interactions,[12−14] ligand acidity,[15] many-body effects,[2,3,16] and solvent isotope effects.[4,5] Recently, the Fe^{2+} ion in aqueous solution has been studied by the Car−Parrinello molecular dynamics technique[17,18] with the focus on chemical reactions in solution. Also very recently, the diffusion properties and librational and vibrational motions of water molecules in the first and second hydration shells of Fe^{2+} and Fe^{3+} were studied by ab initio QM/MM molecular dynamics simulations, where the ions and water molecules inside the first shell were treated quantum-mechanically and those outside it by a force-field method.[19]

Most of the classical simulations have used the Fe^{2+} and Fe^{3+} ion−water potentials developed by Curtiss et al.[2] or Kuharski et al.,[11] combined with rigid-water models (SPC, SPC/E), except for the paper by Floris et al.,[3] in which an effective pair potential based on the polarizable continuum model was used. Flexible-water Fe^{2+}(aq) and Fe^{3+}(aq) simulations have been published by Curtiss et al.,[2] and both rigid- and flexible-water simulations have been published by Guàrdia et al.,[7] who combined the ion−water potential by Curtiss et al. with the SPC[20] and the flexible SPC water models by Toukan and Rahman (SPC-TR)[21] to study the effect of flexibility on the structural and dynamical properties of the solution. Kneifel et al. used both the flexible Bopp−Jancsó−Heinzinger (BJH) water model[22] (in ref 4) and a flexible SPC model (SPC combined with a modified version of the intramolecular part of the BJH model) (in ref 5) in studies that focused on solvent isotope effects.

In the present work, the structure and dynamics of water molecules around the Fe^{2+} and Fe^{3+} ions, as well as the ionic diffusion, are studied using a new flexible water model (SPC+CCL) combined with the ion−water potential by Curtiss et al. We have chosen to describe the iron−water interaction by the existing off-the-shelf effective iron−water potentials by Curtiss et al. because they are known to give good results together with the SPC-based water models. We compare the results using the SPC+CCL model with those from the rigid-body SPC and SPC/E water models. The emphasis in this paper lies on the performance of the new flexible water model. Our study includes an elaborate discussion of the O−H stretching frequency, a property which is most-sensitive to the details of the intra- and intermolecular potentials. The OH stretching frequency of water molecules in the first hydration sphere of trivalent ions is known from experiment to down-shift as much as approximately -850 cm^{-1} compared to the gas-phase value.[23]

The layout of the paper is as follows. The interatomic potentials and the MD simulations are described in the Method section. In the Method section, we also introduce the new flexible-water model used in our simulations. The results are presented and discussed in the Results and Discussion section, where the structural and dynamical properties, as well as the intramolecular vibrations, are reported.

2. Method

2.1. The Interatomic Potentials. Both flexible-water and rigid-water MD simulations were performed. In all cases, the intermolecular ion−water and water−water interactions were described by means of pair-additive potentials.

We have recently constructed a simple flexible-water model, which was found to satisfactorily reproduce many of the properties of pure liquid water, including the OH vibrational band (both its absolute position and its shift with respect to the gas phase[24]). In this model (SPC+CCL), the H_2O-H_2O interactions are expressed as a simple sum of inter- and

* To whom correspondence should be addressed. E-mail: kerst@mkem.uu.se.
[†] Uppsala University.
[‡] Leopold Franzens Universität.

10.1021/jp034855k CCC: $27.50
Published on Web 12/10/2003

intramolecular potentials:

$$\Delta E(H_2O{-}H_2O) = \Delta E^{SPC}(H_2O{-}H_2O) + \Delta E_{intra}(H_2O) \quad (1)$$

Thus, the intermolecular potential is the well-known SPC model and ΔE_{intra} is the quartic potential of Hoy, Mills, and Strey (HMS),[25] as expressed in ρ coordinates by Carney, Curtiss, and Langhoff (CCL)[26] ($\rho = \delta r/r$, $\delta r = r - r_e$). The CCL model is given by

$$U_{intra} = \sum L_{ij}\rho_i\rho_j + \sum L_{ijk}\rho_i\rho_j\rho_k + \sum L_{ijkl}\rho_i\rho_j\rho_k\rho_l \quad (2)$$

where

$$\rho_1^{CCL} = \frac{r_1 - r_e^{CCL}}{r_1} \quad (3)$$

$$\rho_2^{CCL} = \frac{r_2 - r_e^{CCL}}{r_2} \quad (4)$$

and

$$\rho_3^{CCL} = \alpha - \alpha_e \quad (5)$$

and r_1, r_2, and α refer to the two OH bond lengths and the H−O−H angle, respectively. The CCL potential reproduces the gas-phase harmonic frequency at its experimental value, 3890 cm^{-1}.[27] The SPC water molecule has three point masses with an OH distance of 1.00 Å and the HOH angle equal to the tetrahedral angle, while the CCL model has an OH distance of 0.9572 Å and the HOH angle is equal to 104.52°. The SPC oxygen charge is $-0.82e$, and the hydrogen charges are $+0.41e$. Because of the different internal geometries of the two water models, it is not possible to simply connect them.

To graft the CCL potential on the SPC model, it is necessary to establish a correspondence between the internal displacements around the equilibrium positions for the SPC and CCL models. We first rewrite the expressions for the ρ_1^{CCL} and ρ_2^{CCL} coordinates in terms of the Δr^{CCL} displacements around the CCL equilibrium distance; for example, for ρ_1^{CCL},

$$\rho_1^{CCL} = \frac{\Delta r^{CCL}}{\Delta r^{CCL} + r_e^{CCL}} \quad (6)$$

In ref 24, we presented the following coordinate transformation:

$$\rho_1^{SPC+CCL} = \frac{\Delta r^{SPC}}{\Delta r^{SPC} + r_e^{CCL}} = \frac{r_1 - r_e^{SPC}}{r_1 - r_e^{SPC} + r_e^{CCL}} \quad (7)$$

where r_1, again, is the instantaneous OH_1 distance (and similarly for r_2), r_e^{SPC} is the equilibrium distance in the SPC water molecule (1.00 Å), and r_e^{CCL} is the equilibrium distance in the CCL water molecule (0.9572 Å). Because the HOH angle enters in the CCL potential only as an angular displacement around the equilibrium value, the correspondence between the SPC and CCL models is readily made.

Both the Fe^{2+}−water and the Fe^{3+}−water interactions were expressed as pair potentials, taken from Curtiss et al.[2] Originally designed for the flexible SPC-TR water model,[21] these potentials were not modified by us, given the fact that SPC+CCL is closely related to the SPC-TR water model.

Also rigid-water simulations were performed as a comparison of structural and dynamic properties. Here, we used the model of Curtiss et al. combined with the SPC/E water model (extended simple point charge model[28]) because for rigid-water simulations, this model is known to reproduce liquid water properties better than SPC water, especially the dynamical properties.[28] The SPC/E potential was designed for rigid-molecule simulations of pure bulk water[28] and has the same features as SPC, except that it has a charge of $+0.4238e$ on each of the hydrogens and $-0.8476e$ on the oxygen. Rigid-water simulations with the SPC water model were also performed for comparison.

2.2. The MD Simulations. MD simulations with the rigid SPC and SPC/E water models were carried out in the *NPT* ensemble (temperature close to 300 K and zero pressure) with the Nosé−Hoover constant temperature and pressure control[29,30] for both the Fe^{2+}(aq) and Fe^{3+}(aq) solutions. Simulations with the flexible SPC+CCL water model were done in the *NVT* ensemble at a density of 1.000 g cm^{-3}. In all cases, the Coulombic interactions in the system were treated by the Ewald lattice summation method,[31] including the charged system term.[32] The cubic simulation box of ca. 25 Å with periodic boundaries consisted of 512 water molecules and one ion, giving a concentration of 0.11 *m* for both the Fe^{2+} and Fe^{3+} solutions.

For the rigid SPC/E water model, each simulation was equilibrated for about 16 ps, and the data collection was 1.5 ns long with a time step of 1.5 fs. For the rigid-water SPC model, the simulations were run for 600 ps with a time step of 1.5 fs and an equilibration run of 10 ps. For the flexible-water model, each simulation was equilibrated for about 10 ps, and the data collection was at least 200 ps long with a 0.5 fs time step. The molecular coordinates were dumped to disk every 20th time step, except for the part of the simulation (10 ps) that was used for the calculation of the intramolecular vibrations, for which the coordinates were dumped every time step. The drift of the pseudo-Hamiltonian was for all simulations below 1.0% over the whole run.

3. Results and Discussion

3.1. Structural Properties. The local ion hydration structure of each electrolyte solution was analyzed in terms of the ion−oxygen, ion−hydrogen, and oxygen−oxygen radial distribution functions (RDFs), both for the rigid- and for the flexible-water models.

Ion−oxygen and ion−hydrogen RDFs for Fe^{2+}(aq) and Fe^{3+}(aq) have been published earlier,[2−7,18] and our results are in good agreement with these and with extended x-ray absorption fine structure (EXAFS) and neutron diffraction experiments. The ion−oxygen distances fall in the range 2.09−2.28 Å for Fe^{2+}(aq) and 1.98−2.05 Å for Fe^{3+}(aq) (cf. data compilations in ref 1 and 33). Peak positions and coordination numbers for our present study are listed in Table 1. The main features, as shown in Figure 1a,b, are the visible first, second, and third hydration shells (the latter most pronounced for Fe^{3+}), reflecting the long-range ordering of the water molecules by the Fe^{2+} and Fe^{3+} ions. The sharp first ion−oxygen peak indicates a tightly bound first hydration shell, while the deep first minimum down to zero reflects that in both cases none of the six first-shell water molecules exchanges with the second shell during the simulation, consistent with the experimental mean residence times for first-hydration-shell water molecules of 3×10^{-7} s for Fe^{2+} (ref 34) and between 5×10^{-5} (ref 35) and 6×10^{-3} s (ref 36) for Fe^{3+}, as determined by NMR spectroscopy.

TABLE 1: Structural Properties for the First Hydration Shells of the Ferrous and Ferric Ions with the Rigid SPC, Rigid SPC/E, and Flexible SPC+CCL Water Models, Resulting from the Different Radial Distribution Functions[a]

	SPC	SPC/E	SPC+CCL	experiment
		Fe^{2+}(aq)		
R(ion−O)	2.09	2.09	2.09	2.10[33]
R(ion−H)	2.76	2.76	2.4	
R(O···O)[b]	2.74	2.71	2.69	2.76[37]
coordination number	6	6	6	6[33]
		Fe^{3+}(aq)		
R(ion−O)	1.99	1.96	1.96	1.98[33]
R(ion−H)	269	2.66	2.76	
R(O···O)[b]	2.66	2.66	2.63	2.68[23]
coordination number	6	6	6	6[33]

[a] All distances are in Å. [b] R(O···O) refers to the distance between the first and the second hydration shells.

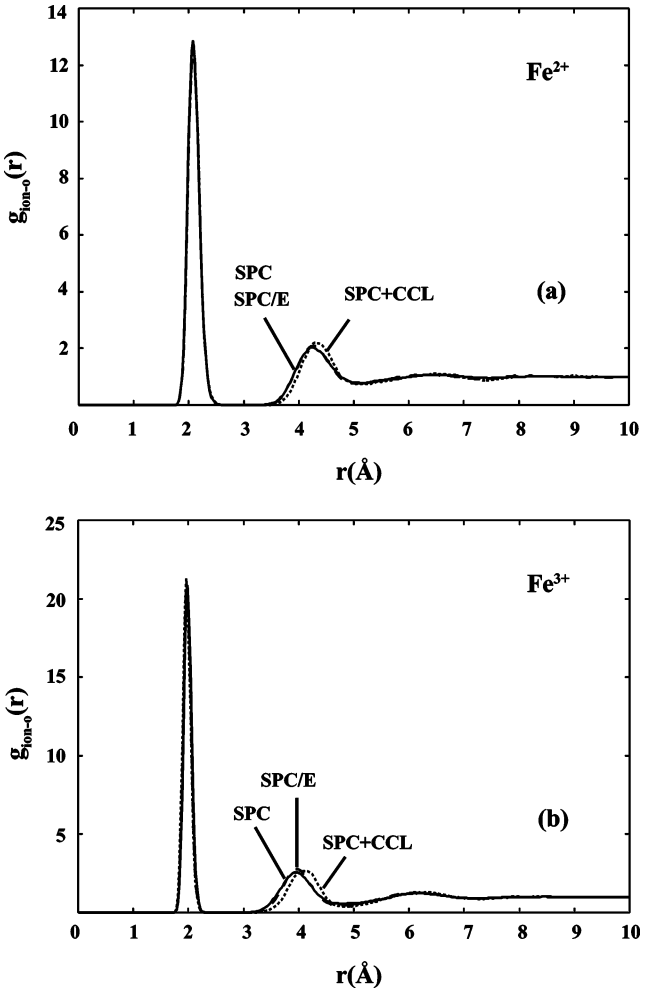

Figure 1. The ion−oxygen radial distribution function for (a) the Fe^{2+} ion and (b) the Fe^{3+} ion with three different water models: SPC (—), SPC/E (− − −), and SPC+CCL (···). For the first peak, the three curves almost completely overlap.

The calculated O···O peak position for the RDF between water molecules in the first and second hydration shells (not shown in Figure 1) is quite close to the experimental value, both for Fe^{2+}(aq) and for Fe^{3+}(aq). The main feature is a sharp peak at ca. 2.71 Å for Fe^{2+} with the three water models and ca. 2.65 Å for Fe^{3+} (see Table 1), indicating a well-ordered first and second hydration shell. This O···O distance is significantly shorter than the average O···O distance in liquid water, which is 2.77, 2.75, and 2.74 Å, respectively, for the SPC, SPC/E, and SPC+CCL models. Experimentally, the O···O distance is 2.86 Å for pure liquid water and 2.76 Å between the first and second hydration shells for Fe^{2+} and 2.68 Å for Fe^{3+}, as derived from frequency−distance correlation curves based on IR experimental data.[37] The simulated shortening thus appears to be too small compared to experiment; a reason may be that the cooperative polarizations between two such water molecules (in the first and second hydration shells, respectively) and the ion in a real ionic solution are not included in our model.

When the solution structures resulting from the three different water models are compared, the conclusion is that the first peak positions for the ion−oxygen and oxygen−oxygen RDFs (not shown here) are not significantly altered by the flexibility (Figure 1). Only the second and third hydration shell peaks are slightly more pronounced in the case of the flexible-water model, indicating a more enhanced water structure. The difference in peak heights between the first and second or third hydration shells are smaller than those found by Guàrdia.[7] Their rigid water−water and ion−water potential parameters are exactly the same as those in our rigid SPC simulation, but their MD box size, their thermostat, and their treatment of the long-range interactions were different. The peak in the ion−hydrogen RDF (not shown here) is shifted to the right for the flexible-water model compared to the rigid models, a result of the lengthening of the O−H bond (see section 3.4.1). For all three water models and for both ions, we obtain a coordination number of 6 for the first shell. The second-shell coordination numbers are found in the range 10−15 with an average of 12 for both ions in the case of the SPC and SPC/E simulations and an average of 12 for Fe^{2+} and 12.5 for Fe^{3+} in the case of the SPC+CCL simulations.

The shorter ion−oxygen distance of 1.963 Å for Fe^{2+} compared to 2.088 Å for Fe^{3+}, as expected from the different ionic radii, and a slightly narrower and much higher first-shell ion−water peak for Fe^{3+}, and also (slightly) higher second- and third-shell peaks for Fe^{3+}, are the most important structural differences between Fe^{2+} and Fe^{3+} visible in Figure 1. A higher peak value for the oxygen−oxygen RDF between the first and second hydration shells (not shown here) in the case of Fe^{3+} compared to Fe^{2+} is also noteworthy, an indication of a more-ordered second shell.

3.2. Transport Properties. The translational motion of ions and solvent molecules was analyzed in terms of the mean-square displacement (MSD), and the self-diffusion coefficient D was calculated from the Einstein relation[38]

$$D = \frac{1}{6}\lim_{t\to\infty}\frac{\mathrm{d}}{\mathrm{d}t}\mathrm{MSD}(t) = \frac{1}{6}\lim_{t\to\infty}\frac{\mathrm{d}}{\mathrm{d}t}\langle|\vec{r}(t_0+t)-\vec{r}(t_0)|^2\rangle \qquad (8)$$

where the average is taken over time origins and molecules. D was in each case obtained from a least-squares fit from 1 to 5 ps. The diffusion coefficient was calculated for the ion and for four different groups of water molecules: (i) first hydration shell, (ii) second hydration shell, (iii) third hydration shell, and (iv) bulk water molecules. The group identification was based on the ion−oxygen RDFs. The same groups of water molecules will also be used in the discussion in section 3.2. For the diffusion coefficient, the classification was done at $t = 0$ ps, that is, if a molecule changes groups between t = 0 and 5 ps, the group at $t = 0$ ps was used in the classification. The resulting diffusion coefficients with their uncertainties are collected in Table 2 for the six MD simulations, together with the experimental values. Here, the standard error of the mean is estimated from averages after dividing the data into independent blocks (see, for example, ref 39).

TABLE 2: Self-Diffusion Coefficients (in 10^{-5} cm^2 s^{-1}) Obtained from the MD Simulations with the Rigid SPC, Rigid SPC/E, and Flexible SPC+CCL Water Models

	SPC	SPC/E	SPC+CCL	experiment
		Fe^{2+}(aq)		
Fe^{2+} ion	0.93(3)	0.56(4)	0.53(5)	0.70, 0.64[41,42]
1st shell water	1.45(1)	0.72(4)	0.69(5)	
2nd shell water	3.32(11)	1.95(3)	1.94(12)	
3rd shell water	3.81(9)	2.39(3)	2.30(9)	
bulk water	4.09(5)	2.55(1)	2.52(5)	
		Fe^{3+}(aq)		
Fe^{3+} ion	0.71(6)	0.53(2)	0.43(7)	0.55, 0.53, 0.68[42,43,44]
1st shell water	0.90(6)	0.65(2)	0.58(5)	
2nd shell water	2.35(7)	1.64(3)	1.59(2)	
3rd shell water	3.84(3)	2.29(3)	2.33(8)	
bulk water	4.07(4)	2.54(3)	2.58(5)	
pure water	4.30[27]	2.50[27]	2.55(4)	2.40[59]

The residence time correlation function has been calculated according to

$$R(t) = \frac{1}{N}\sum_{i=1}^{N}\langle\theta_i(t)\theta_i(0)\rangle^2 \qquad (9)$$

following the method described in ref 40. Here θ is the Heaviside unit step function, which is 1 if the water molecule is in the hydration shell of the ion at time t and zero otherwise, and N is the hydration number of the shell. We allow for a temporary excursion time of 2 ps. The residence time τ for a water molecule in the second hydration shell was calculated by fitting the entire residence time correlation function to an exponential of the form $e^{-t/\tau}$.

The self-diffusion coefficients for the Fe^{2+} and Fe^{3+} ions are $0.56(4) \times 10^{-5}$ and $0.53(5) \times 10^{-5}$ cm^2 s^{-1}, respectively, for the SPC/E water model and $0.53(2)$ and $0.43(7) \times 10^{-5}$ cm^2 s^{-1} for the flexible model, that is, very close to one another (Table 2). The results of the simulation are in good agreement with the experimental self-diffusion coefficients for the Fe^{2+} and Fe^{3+} ion in acidified solutions, as determined by the tracer diffusion method. These values lie in the range $(0.64-0.70) \times 10^{-5}$ cm^2 s^{-1} for Fe^{2+} [41,42] and $(0.53-0.68) \times 10^{-5}$ cm^2 s^{-1} for Fe^{3+} [42-44] and are thus very similar for the two ions. All of these experimental diffusion coefficients were measured in 0.1 *m* solutions, except for the Fe^{3+}(aq) value in ref 44, which was obtained from measurements for a concentrated (2.0 *m*) solution. Our theoretical results also suggest that the diffusion coefficient for Fe^{3+} is the same as that for Fe^{2+} within statistical error, although the structural simulation results indicate slightly more strongly bound water molecules in the case of Fe^{3+}.

Within statistical error, the first-shell water molecules diffuse along with the ion, that is, both ions have the same (effective) coordination number, which is reflected in the similarity of the diffusion coefficients here. The values for the diffusion coefficient of the Fe^{2+} and Fe^{3+} ions with the SPC water model, 0.93×10^{-5} and 0.71×10^{-5} cm^2 s^{-1}, are overestimated compared to experiment and show once more the sensitivity of the dynamical properties to the description of the electrostatics in the different models[28] (i.e., the increased average dipole moment of the SPC/E and SPC+CCL models compared to SPC). The dynamics for the SPC water model is too fast, which is also reflected in the residence times for the water molecules in the second hydration shell. The excessive dynamics for the SPC water model is well-known from the literature for pure liquid water (cf. the last row of Table 2).

The diffusion coefficient of water molecules in the second shell holds an intermediate position between the bulk waters and the strongly bound first hydration shell waters. This is due to the exchange between the second shell water molecules and the bulk via the third shell; this exchange is quantified by the mean residence times of the second-shell water molecules displayed in Table 3 for the rigid-water and the flexible-water models. The difference in diffusion coefficient for the water molecules in the second shell around the two ions should, at least partly, be related to the difference in residence times for the second shell water molecules around the ions. The residence time around Fe^{3+} lies in the range 25-28 ps (depending on the model, excluding the SPC model for reasons given above), almost twice as long as that for Fe^{2+}, and this results in a lower diffusion coefficient for water molecules in the second shell around Fe^{3+}. For the third-shell water molecules, we can safely assume that they exhibit quite bulklike dynamical behavior.

TABLE 3: Residence Times, τ (ps), for the Water Molecules in the Second Hydration Shell Calculated as Described in the Text from the MD Simulations with the Rigid SPC, Rigid SPC/E, and Flexible SPC+CCL Water Models

	SPC	SPC/E	SPC+CCL
Fe^{2+}(aq)	10.1	15.3	13.9
Fe^{3+}(aq)	17.4	27.7	25.0

TABLE 4: Average Intramolecular Water Geometry (in Å and deg) Obtained from the MD Simulations with the Flexible SPC+CCL Water Model[a]

	Δr(OH)	ΔHOH angle (deg)
	Fe^{2+}(aq)	
1st shell water	+0.034	−7.5
2nd shell water	+0.021	−4.8
3rd shell water	+0.022	−4.8
bulk water	+0.009	−4.8
pure water	+0.007	−4.4
	Fe^{3+}(aq)	
1st shell water	+0.057	−10.5
2nd shell water	+0.022	−5.1
3rd shell water	+0.022	−4.8
bulk water	+0.009	−4.8
pure water	+0.007	−4.4

[a] The gas-phase r(OH) value for SPC water is 1.000 Å, and the H−O−H angle is 109.47°. Δr(OH) and ΔHOH angle are listed with respect to these values.

3.3. Intramolecular Geometry. Before presenting the analysis of the O−H vibrational spectra, we discuss the intramolecular geometry of the water molecules. The presence of a polyvalent cation leads to a strong distortion of the surrounding water molecules. Experimental evidence from studies in the crystalline state[45] and ab initio calculations (e.g., see ref 46) shows that, because of the environment, the OH bonds of bound water molecules are significantly elongated compared to the isolated water molecule. The geometric distortions of the solvent molecules caused by the cations have also been observed in MD simulations of aqueous ionic solutions:[47,48] first the lengthening of the O−H bond, already briefly mentioned in the structural properties section, and, second, a closing of the HOH angle. The lengthening of the O−H bond and the closing of the HOH angle were observed in the previous MD simulations of Fe^{2+} and Fe^{3+} with flexible-water models in refs 5 and 19 but not in refs 4 and 7.

In the present work, the O−H bond lengths and HOH angles have been computed for the four previously defined water types and are listed in Table 4. Obviously, the geometric distortions are the most dramatic for the first water shell, where we find that the O−H bond length increases by, on average, 0.015 and

0.036 Å for Fe^{2+} and Fe^{3+}, respectively, compared to pure liquid water; the effect decreases when moving further away from the ion. These shifts are in agreement with experimentally observed increased O−H bond lengths for $Mg(H_2O)_6^{2+}$ in solution (r_{OH} = 0.996 Å) and $Al(H_2O))_6^{3+}$ in solution (r_{OH} = 1.019 Å), as determined by NMR,[49] compared to that of liquid water at 298 K (r_{OH} = 0.96 Å),[50] as determined by neutron diffraction. The experimental OH distance shifts are rather uncertain, however, not least because a liquid-phase value of 0.96 Å must be too short, because the OH distance for a water molecule in the gas phase has been determined to 0.971 Å[51] (equilibrium structure with zero-point vibrational correction) and the OH bond in the liquid phase is expected to be elongated with respect to the gas phase. MD simulations of $Be^{2+}(aq)$[47] and $AlCl_3(aq)$[48] gave the result that the OH bond for the first-shell water molecules around Be^{2+} and Al^{3+} were elongated by 0.049 and 0.070 Å, respectively, compared to the free water molecule.

The bond angle changes significantly only for the first-shell water molecules, a decrease of 7.5° for Fe^{2+} and of 10.5° for Fe^{3+}. In the case of Be^{2+} [47] and Al^{3+} [48], the water angle was found to decrease by 10° and 15°, respectively (MD simulations). The closing of the water angle appears to be in contrast with the average situation in the ionic crystalline hydrates, for which the average H−O−H angle has been determined from neutron diffraction studies to be 2.5° larger than the gas-phase value,[45] and with results from Car−Parrinello work by Marx et al.,[52] who found an increased HOH angle in the first hydration shell of Be^{2+}.

The lengthening of the O−H bond and the closing of the HOH angle are not completely correlated in our results. The closing of the angle is only significant for the first-shell waters, while the lengthening of the O−H bond reaches as far out as the third shell, a zone where the transport properties are almost bulklike. This effect seems to be independent of the charge of the ion; for Fe^{2+} and Fe^{3+}, we obtain the same elongation for the water molecules, in both the second and third shells (within statistical error).

3.4. Vibrational Spectra.

3.4.1. Three Types of Spectra. Vibrational spectroscopy is a well-established method for the investigation of solute hydration. More specifically, the OH vibrations appear to be a most-sensitive and well-suited probe for ionic hydration. For liquid water, the experimentally determined OH stretching frequency, that is, the "band origin" of the rather broad OH band, occurs at ∼3400 cm^{-1},[53] that is, it is downshifted by ca. 300 cm^{-1} compared to the average value of the antisymmetric and the symmetric OH vibrations of the isolated gas-phase H_2O molecule (symmetric, 3657 cm^{-1}; antisymmetric, 3756 cm^{-1}; average, 3707 cm^{-1} [54]). The influence of multivalent ions on their surrounding water molecules results in even larger OH frequency downshifts. Here, three different types of intramolecular vibrational OH spectra were calculated: a "classical" VAC-FT spectrum, a "quantum-mechanical" anharmonic spectrum, and a truly "harmonic" spectrum, the latter two by means of a frozen-field approach. The anharmonic spectra are quantum-mechanical in the sense that the nuclear motion is treated quantum-mechanically (see below).

The "classical" VAC-FT spectra of the O−H vibrational frequencies for the four types of water molecules defined above were calculated by taking the Fourier transform of the velocity autocorrelation function (VAC) for the relative velocities of the H atoms with respect to the velocity of the O atom. Each spectrum shows two peaks: the first one around 1700 cm^{-1} (not shown here) due to the HOH bending vibration and, higher up in frequency, the broad O−H stretching band (Figure 3).

For the calculation of the *anharmonic quantum-mechanical spectrum*, we started from the MD configurations. To avoid the complications arising from the vibrational couplings between the OH oscillators, we here considered the vibrations of isotopically isolated HDO molecules, following the approach outlined in ref 55. Although the MD simulations were performed with H_2O, such a procedure is valid because the frequency for the one-legged OH vibration in HDO falls at the same value as the average of the symmetric and antisymmetric OH vibrations in H_2O. In ref 55 and here, the internal stretching vibrations of each water molecule were calculated in the field of all of the other distorted water molecules surrounding this molecule. The surrounding molecules were assumed to be fixed and form a so-called "frozen field" around the vibrating molecule. For each water molecule, we calculated the OH stretching potential energy curve using the SPC+CCL potential for the water−water interactions and the Curtiss potential for the ion−water interactions, and we kept the HDO angle and the water center-of-mass fixed to mimic the OH normal mode in HDO. The potential curve was expanded in a Taylor series, and the r_e value and force constants were determined by least-squares fitting. The Schrödinger equation for the motion of the proton in this potential was solved variationally, and the anharmonic frequencies were calculated from the resulting eigenlevels. The frequencies of the water molecules were collected in density-of-states histograms. Details of this whole procedure can be found in refs 56 and 46.

The harmonic spectrum was also generated from the OH potential curves calculated for the MD solution snapshots, as described above. However, this time only the second derivative of each curve was used to provide the harmonic force constant at the minimum of each curve and from this the harmonic frequency. The frequencies were collected into density-of-states histograms to produce the harmonic spectrum.

Among the three types of spectra that we compute, it is the anharmonic quantum-mechanical spectrum that is of the highest quality and that, in case of a sufficiently good force-field, should yield vibrational frequency band maxima in agreement with experiment.

3.4.2. Pure Liquid Water. The simulated spectra (classical, anharmonic, harmonic) for pure liquid water using the SPC+CCL water model are shown in Figure 2a. Table 5 lists the frequency values for the peak maxima. The band maxima of the classical VAC and the harmonic spectra almost coincide because only the bottom part of the potential is sampled in a classical MD simulation and the anharmonic part of the OH stretching potential is insufficiently sampled.[46,56] As a result, there is only a small difference between the two spectra: the peak maximum falls at 3590 cm^{-1} for the classical spectrum and at 3610 cm^{-1} for the harmonic spectrum. The calculated anharmonic vibrational frequency, on the other hand, lies at 3420 cm^{-1}, close to experiment. Experimentally, the downshift of bulk water compared to the isolated water molecule is 300 cm^{-1}.[57] All of our computed downshifts are close to this value; we find a downshift of 300 cm^{-1} for the classical spectrum, 300 cm^{-1} for the anharmonic spectrum, and 280 cm^{-1} for the harmonic spectrum. The combination of the SPC intermolecular and the CCL intramolecular potential thus results in absolute and relative spectral positions in very good agreement with experiment for pure liquid water. This is a reliable starting point for our study of the influence of the ferrous and ferric ions on the OH stretching band for the water molecules around the ions.

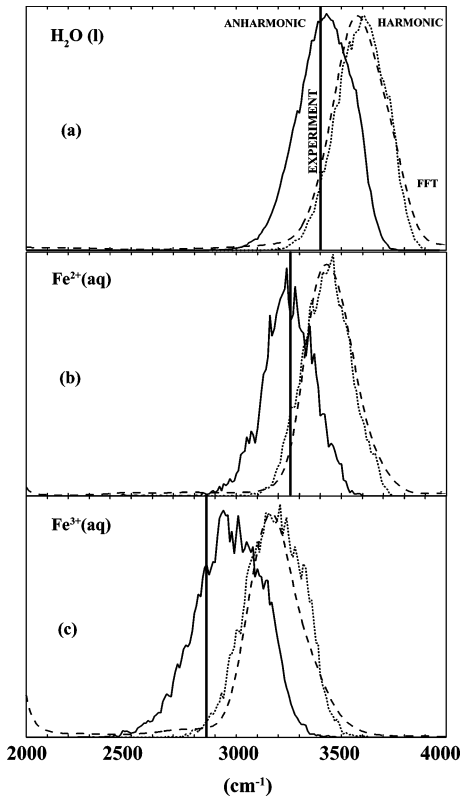

Figure 2. The three calculated OH stretching spectra, that is, the quantum-mechanical anharmonic frozen-field spectrum (—), the harmonic frozen-field spectrum (•••), and the classical FT spectrum (– – –), together with the experimental value indicated by a vertical line. (a) For pure liquid water, (b) for the water molecules in the first hydration shell of the Fe^{2+} ion, and (c) for the water molecules in the first hydration shell of the Fe^{3+} ion. See text for details concerning potentials and computational strategy for the three types of spectra.

TABLE 5: Positions of the Peak Maxima for the OH Stretching Bands (in cm^{-1}) Calculated for the First Shell Water Molecules around Fe^{2+}(aq) and Fe^{3+}(aq)[a]

			frozen-field spectra						
	FT of VAC		harmonic		anharmonic		experimental		
	"ω"	"$\Delta\omega$"	ω	$\Delta\omega$	ν	$\Delta\nu$	ν	$\Delta\nu$	ref
H_2O(g)[b]	3890		3890		3720		3707		52
H_2O(l)	3590	−300	3610	−280	3420	−300	3400	−310	51
Fe^{2+}(1st shell)	3420	−470	3450	−440	3280	−440	3250	−460	37
Fe^{3+}(1st shell)	3160	−730	3150	−740	−940	−760	2850	−860	23

[a] Frequency shifts are listed with respect to the isolated gas-phase molecule. The SPC+CCL water−water model was used in all cases. "FT of VAC" means according to formula 4 in the text, and the frequencies are denoted "ω" because the method essentially yields the harmonic OH frequency (see text). [b] The average of the symmetric and antisymmetric OH stretching vibrational frequencies or, equivalently, the frequencies for the OH stretching vibration in the isotope-isolated HDO molecule.

3.4.3. Fe^{2+}(aq) and Fe^{3+}(aq). Infrared spectroscopic data is available for dilute aqueous Fe^{2+} solutions.[37] For Fe^{3+}, there are no data available, but experimental IR results for other trivalent cations, such as Al^{3+}, Cr^{3+}, and Rh^{3+}, exist.[23] Experimental IR double-difference spectra were measured by Bergström et al.[23] for water molecules in the first hydration spheres of Fe^{2+} and Al^{3+} and show bands centered around 3260 and 2850 cm^{-1}, respectively; that is, they are downshifted by as much as 450 and 860 cm^{-1} compared to the average gas-phase water OH stretching frequency at 3707 cm^{-1}.

Our calculated spectra for the first-shell water molecules around the ferrous and ferric ion are shown in Figure 2b,c, and the peak positions are listed in Table 5. For the Fe^{2+} ion, the calculated anharmonic spectrum lies at 3280 cm^{-1}, that is, very close to the experimental value. The classical and harmonic spectra are found close to each other and lie at 3420 and 3450 cm^{-1}, respectively. Our calculated absolute frequencies correspond to downshifts (with respect to the isolated water molecule) of 440 cm^{-1} for the anharmonic spectrum and 440−470 cm^{-1} for the harmonic and classical spectra, that is, in very good agreement with the experimental downshift of 450 cm^{-1}. The simulation results by Kneifel et al.[5] for the water molecules around Fe^{2+} and Fe^{3+}, 3305 and 2675 cm^{-1}, respectively, should be compared with the "experimental" values for the harmonic frequencies, which would lie ca. 200 cm^{-1} above the measured anharmonic frequencies, that is, at ∼3460 cm^{-1} for Fe^{2+}(aq) and ∼3050 cm^{-1} for Fe^{3+}(aq). The vibrations of Kneifel et al. are thus too much downshifted in frequency, especially in the case of Fe^{3+}. The frequencies from the QM/MM MD simulations by Remsungnen et al.[19] for the first hydration sphere around the ferrous and ferric ions are blue-shifted with respect to pure liquid water, in contrast to experiment. We can conclude that the empirical pair potential by Curtiss et al. in combination with the SPC+CCL potential performs remarkably well in the description of the ion−water interaction in Fe^{2+}(aq) and its effect on the OH frequencies.

For the Fe^{3+} ion, the calculated first-shell anharmonic OH spectrum lies at 2940 cm^{-1}, about 100 cm^{-1} higher than its experimental value. For the very strongly polarized water molecules around Fe^{3+}, our description of the ion−water interaction by means of empirical pair potentials is expected to be less accurate. In view of the fact that the experimental downshift is as large as 850 cm^{-1}, our computed downshift of 760 cm^{-1} must be considered quite satisfactory, only 10% too small.

For the water molecules in the second and third hydration spheres and in the bulk, we have calculated the classical OH spectrum from the MD simulations. The water molecules in the second shell give rise to a band around 3560 cm^{-1} for both ions, corresponding to a small downshift of 30 cm^{-1} with respect to the calculated value for pure liquid water at 3590 cm^{-1} (see Table 5). Comparison with experimental IR data for Al^{3+}(aq)[23] suggests that for the second-shell water molecules around Fe^{3+} this downshift of 30 cm^{-1} is too small. The similarity of the second-shell OH frequencies for Fe^{2+} and Fe^{3+} ions is consistent with the very similar lengthenings found for these OH bonds, as discussed above, because both from experiments and calculations the quantities Δr_e and $\Delta\nu$ are known to be very strongly correlated. The OH frequencies for the water molecules in the third shell and in "the bulk" lie close to pure water at 3370 cm^{-1} (only 20 cm^{-1} off). We conclude that this ion−water potential yields downshifts that are smaller than the experimental shifts for the water molecules in the second hydration sphere.

The water bending frequency is up-shifted for the water molecules in the first hydration shell; for Fe^{2+} and Fe^{3+}, we find peak maxima of 1810 and 1760 cm^{-1}, respectively, and the shifts with respect to pure liquid water are 50 and 100 cm^{-1}. Such upshifts were also observed by Guàrdia et al.,[7] while no significant shift was found by Kneifel et al.[4] The bending frequencies for the second and third shells and for bulk water molecules lie at ca. 1710 cm^{-1}, equal to the value for pure liquid water (the experimental value is 1645 cm^{-1} [58]).

Conclusions

In the present MD simulations of Fe^{2+} and Fe^{3+}, we have compared three different SPC-based water models combined

with an empirical pair potential for the ion−water interactions. From our comparison, we can draw the following conclusions. As far as the structural properties are concerned, we find that for the three water models used (SPC, SPC/E, and SPC+CCL) three clearly visible hydration shells emerge, reflecting long-range ordering due to the presence of the ions and with all features more clearly marked in the case of the more highly charged Fe^{3+} ion. The structural differences between the models are rather small; they essentially show up in the ion−hydrogen and the first to second shell oxygen−oxygen radial distribution functions for the flexible-water model compared to those of the two rigid models.

The dynamical properties of the solutions are very sensitive to the description of the electrostatics in the different water models. Thus, for SPC/E and SPC+CCL, we obtain ionic self-diffusion coefficients in agreement with experimental values but not for SPC. The diffusion coefficients for Fe^{2+} and Fe^{3+} are very similar. The influence of the ions on the dynamical properties reaches out to the second hydration shell for both ions.

With regard to the flexible-water simulations, we can conclude the following. The SPC+CCL flexible-water model can accurately reproduce the OH stretching frequencies for liquid water and provides a reliable starting point to study the influence of the ions on the vibrational spectra. The combination of SPC+CCL with the empirical pair potential from Curtiss et al.[2] appears to work well for the computation of the intramolecular stretching frequencies (as well as the structural and dynamical properties). Both the absolute frequencies and the frequency shifts from our simulations reproduce the experimental data well.

In summary, we find that the flexible-water model SPC+CCL describes the structural properties and the diffusion equally well or better than the SPC/E water model for the Fe^{2+}(aq) and Fe^{3+}(aq) solutions. In addition, it yields OH vibrational frequencies in good agreement with experiment.

Acknowledgment. This work has been supported by the Swedish Science Council (VR) and the European FP5 IHP program (Research Training Network Contract No. HPRN-CT-2000-19).

References and Notes

(1) Ohtaki, H.; Radnai, T. *Chem. Rev.* **1993**, *93*, 1157.
(2) Curtiss, L. A.; Hallay, J. W.; Hautman, J.; Rahman, A. *J. Chem. Phys.* **1987**, *86*, 2319.
(3) Floris, F.; Persico, M.; Tani, A.; Tomasi, J. *Chem. Phys. Lett.* **1992**, *199*, 518.
(4) Kneifel, C. L.; Friedman, H.; Newton, M. D. *Z. Naturforsch.* **1989**, *44a*, 385.
(5) Kneifel, C. L.; Newton, M. D.; Friedman, H. L. *J. Mol. Liq.* **1994**, *60*, 107.
(6) Degrève, L.; Quintale, C., Jr. *J. Electroanal. Chem.* **1996**, *409*, 25.
(7) Guàrdia, E.; Padró, J. A. *Chem. Phys.* **1990**, *144*, 353.
(8) Rustad, J. R.; Hay, B. P.; Halley, J. W. *J. Chem. Phys.* **1995**, *102*, 427.
(9) González-Lafont, A.; Llunch, J. M.; Oliva, A.; Bertrán, J. *J. Comput. Chem.* **1991**, *12*, 1165.
(10) Friedman, H. L.; Newton, M. D. *J. Electrochem. Soc.* **1987**, *134*, 138.
(11) Kuharski, R. A.; Bader, J. S.; Chandler, D.; Sprik, M.; Klein, M. L.; Impey, R. W. *J. Chem. Phys.* **1989**, *89*, 3248.
(12) Bader, J. S.; Chandler, D. *J. Phys. Chem.* **1992**, *96*, 6423.
(13) Kumar, P. V.; Tembe, B. L. *J. Chem. Phys.* **1992**, *97*, 4356.
(14) Babu, C. S.; Madhusoodanan, M.; Sridhar, G.; Tembe, B. L. *J. Am. Chem. Soc.* **1997**, *119*, 5679.
(15) Chang, C. M.; Wang, M. K. *Chem. Phys. Lett.* **1998**, *286*, 46.
(16) Curtiss, L. A.; Hallay, J. W.; Hautman, J. *Chem. Phys.* **1989**, *133*, 89.
(17) Ensing, B.; Baerends, E. J. *J. Phys. Chem. A* **2002**, *106*, 7902.
(18) Ensing, B.; Buda, F.; Blöchl, P. E.; Baerends, E. J. *Phys. Chem. Chem. Phys.* **2002**, *4*, 3619.
(19) Remsungnen, T.; Rode, B. M. *Chem. Phys. Lett.* **2003**, *367*, 586.
(20) Berendsen, H. J.; Postma, J. P. M.; van Gunsteren, W. F.; Hermans, J. In *Intermolecular Forces*; Pullman, B., Ed.; Reidel: Dordrecht, The Netherlands, 1981.
(21) Toukan, K.; Rahman, A. *Phys. Rev. B* **1985**, *31*, 2643.
(22) Bopp, P.; Jancsó, G.; Heinzinger, K. *Chem. Phys. Lett.* **1983**, *98*, 129.
(23) Bergström, P.-A.; Lindgren, J.; Read, M.; Sandström, M. *J. Phys. Chem.* **1991**, *95*, 7650.
(24) Amira, S.; Spångberg, D.; Hermansson, K., to be submitted for publication.
(25) Hoy, A. R.; Mills, I. M.; Strey, G. *Mol. Phys.* **1972**, *24*, 1265.
(26) Carney, G. D.; Curtiss, L. A.; Langhoff, S. R. *J. Mol. Spectrosc.* **1976**, *61*, 371.
(27) Bartlett, R.; Cole, S. J.; Purvis, G.; Ermler, W. C.; Hsieh, H. C.; Shavitt, I. *J. Chem. Phys.* **1987**, *87*, 6579.
(28) Berendsen, H. J. C.; Grigera, J. R.; Straatsma, T. P. *J. Phys. Chem.* **1987**, *91*, 6269.
(29) Nosé, S. *Mol. Phys.* **1984**, *52*, 255.
(30) Hoover, W. G. *Phys. Rev.* **1985**, *A31*, 1695.
(31) Allen, M. P.; Tildesley, D. J. *Computer Simulations of Liquids*; Clarendon Press: Oxford, U.K., 1987.
(32) Hummer, G.; Pratt, L. R.; García, A. E. *J. Phys. Chem.* **1996**, *100*, 1206.
(33) Brunschwig, B. S.; Creutz, C.; Macartney, D. H.; Sham, T. K.; Sutin, N. *Faraday Discuss. Chem. Soc.* **1982**, *74*, 113.
(34) Swift, T. J.; Coninck, R. E. *J. Chem. Phys.* **1962**, *37*, 307.
(35) Fiat, D.; Coninck, R. E. *J. Am. Chem. Soc.* **1968**, *90*, 608.
(36) Grant, M.; Jordan, R. B. *Inorg. Chem.* **1981**, *20*, 55.
(37) Kristiansson, O.; Eriksson, A.; Lindgren, J. *Acta Chem. Scand.* **1984**, *A38*, 613.
(38) Einstein, A. *Ann. Phys.* **1905**, *17*, 549.
(39) Rey, R. *J. Chem. Phys.* **1996**, *104*, 1966.
(40) Impey, R. W.; Madden, P. A.; McDonald, I. R. *J. Phys. Chem.* **1983**, *87*, 5071.
(41) Price, W. E.; Woolf, L. A. *J. Solution Chem.* **1992**, *21*, 239.
(42) Reiners, G.; Lorenz, W. J.; Hertz, H. G. *Ber. Bunsen-Ges. Phys. Chem.* **1978**, *82*, 738.
(43) Easteal, A. J.; Malhotra, R.; Price, W. E.; Woolf, L. A. *J. Solution Chem.* **1991**, *20*, 319.
(44) Herman, G. J.; Salmon, P. S. *J. Am. Chem. Soc.* **1991**, *113*, 2930.
(45) Chiari, G.; Ferraris, G. *Acta Crystallogr. B* **1982**, *38*, 2331.
(46) Ojamäe, L.; Hermansson, K. *J. Chem. Phys.* **1992**, *96*, 9035.
(47) Probst, M. M.; Spohr, E.; Heinzinger, K. *Mol. Simul.* **1991**, *7*, 43.
(48) Lauenstein, A.; Hermansson, K.; Lindgren, J.; Probst, M.; Bopp, P. *Int. J. Quantum Chem.* **2000**, *80*, 892.
(49) van der Maarel, J. R. C.; de Boer, H. R. W.; de Bleijser, J.; Bedeaux, D.; Leyte, J. C. *J. Chem. Phys.* **1987**, *86*, 3373.
(50) Soper, A. K. *Chem. Phys.* **2000**, *258*, 121.
(51) Kuchitsu, K.; Bartell, L. S. *J. Chem. Phys.* **1962**, *36*, 2460.
(52) Marx, D.; Sprik, M.; Parrinello, M. *Chem. Phys. Lett.* **1997**, *237*, 360.
(53) Wyss, H. R.; Falk, M. *Can. J. Chem.* **1970**, *48*, 607.
(54) Darling, B. T.; Dennison, D. M. *Phys. Rev.* **1940**, *57*, 128.
(55) Wojcik, M. J.; Lindgren, J. *Chem. Phys. Lett.* **1983**, *99*, 116.
(56) Hermansson, K.; Knuts, S.; Lindgren, J. *J. Chem. Phys.* **1991**, *45*, 7486.
(57) Benedict, W. S.; Gailar, N.; Plyler, E. K. *J. Chem. Phys.* **1956**, *24*, 1139.
(58) Eisenberg, D.; Kauzman, W. *The Structure and Properties of Water*; Oxford University Press: London, 1969.
(59) Krynicki, K.; Green, C. D.; Sawyer, D. W. *Faraday Discuss.* **1978**, *66*, 199.